CCDC113 stabilizes sperm axoneme and head-tail coupling apparatus to ensure male fertility

Bingbing Wu[1,2,3#], Chenghong Long[1#], Yuzhuo Yang[4,5], Zhe Zhang[4,5], Shuang Ma[1,2,3], Yanjie Ma[1,2,3], Huafang Wei[1], Jinghe Li[1], Hui Jiang[4,5], Wei Li[1,2,3*], Chao Liu[1,2,3*]

[1] Guangzhou Women and Children's Medical Center, Guangzhou Medical University, Guangzhou 510623, China.

[2] State Key Laboratory of Stem Cell and Reproductive Biology, Institute of Zoology, Stem Cell and Regenerative Medicine Innovation Institute, Chinese Academy of Sciences, Beijing 100101, China.

[3] University of Chinese Academy of Sciences, Beijing 100049, China.

[4] Department of Urology, Department of Reproductive Medicine Center, Peking University Third Hospital, Beijing 100191, China.

[5] Department of Urology, Peking University First Hospital Institute of Urology, Peking University, Beijing 100034, China

[#] These authors contributed equally to this work.

[*]Corresponding Authors:

Dr. Wei Li

Guangzhou Women and Children's Medical Center,

No. 9 Jinsui Road, Tianhe District,

Guangzhou 510623, China.

Email: leways@gwcmc.org

Dr. Chao Liu

Guangzhou Women and Children's Medical Center,

No. 9 Jinsui Road, Tianhe District,

Guangzhou 510623, China.

Email: liuchao@gwcmc.org

Abstract

The structural integrity of the sperm is crucial for male fertility, defects in sperm head-tail linkage and flagellar axoneme are associated with acephalic spermatozoa syndrome (ASS) and the multiple morphological abnormalities of the sperm flagella (MMAF). Notably, impaired head-tail coupling apparatus (HTCA) often accompanies defects in the flagellum structure, however, the molecular mechanisms underlying this phenomenon remain elusive. Here, we identified an evolutionarily conserved coiled-coil domain-containing (CCDC) protein, CCDC113, and found the disruption of CCDC113 produced spermatozoa with disorganized sperm flagella and HTCA, which caused male infertility. Further analysis revealed that CCDC113 could bind to CFAP57 and CFAP91, and function as an adaptor protein for the connection of radial spokes, nexin-dynein regulatory complex (N-DRC) and doublet microtubules (DMTs) in sperm axoneme. Moreover, CCDC113 was identified as a structural component of HTCA, collaborating with SUN5 and CENTELIN to connect sperm head to tail during spermiogenesis. Together, our studies reveal that CCDC113 serve as critical hub for sperm axoneme and HTCA stabilization, providing insights into the potential pathogenesis of infertility associated with human CCDC113 mutations.

Keywords: CCDC113, male infertility, HTCA formation, axoneme stabilization, radial spoke

Introduction

The integrity of spermatozoa is necessary for its migration through the female reproductive tract and successful fertilization, and an intact spermatozoon contains proper sperm head, head-tail coupling apparatus (HTCA), and flagellum (Parker, 2020; Roldan, 2019). Many components have been identified in sperm HTCA or flagellum, and are essential for the sperm integrity (Lehti & Sironen, 2017; Wu et al., 2020). Defects in sperm flagellum and HTCA may lead to reduced sperm motility or aberrant sperm morphology, termed as multiple morphological abnormalities of the sperm flagella (MMAF) or acephalic spermatozoa syndrome (ASS), in turn, which causes male infertility (Sudhakar et al., 2021; Tu et al., 2020).

Sperm flagellum possesses an evolutionarily conserved axonemal structure composed of "9+2" microtubules, specifically, nine peripheral doublet microtubules (DMTs) surrounding two central microtubules known as the central pair (CP) (Inaba & Mizuno, 2016). Axonemal dyneins, radial spokes (RS), and the nexin-dynein regulatory complex (N-DRC), are arranged on DMTs with a 96-nm repeating unit structures (Kumar & Singh, 2021). In axoneme, the N-DRC and RS are required for axonemal integrity, which form a crossbridge between neighboring DMTs and link the DMTs to the central apparatus, respectively (Canty et al., 2021; Ishikawa, 2017; Kumar & Singh, 2021). Recent advances in artificial intelligence, biochemical techniques, and cryo-electron microscopy (cryo-EM) facilitated the analysis of the axonemal structures, and numerous components were detected among RS, N-DRC and DMTs, which may serve as hubs to stabilize the axoneme (Bazan et al., 2021; Leung et al., 2023; Walton et al., 2023; Zhou et al., 2023). Such as, CFAP91 is identified to extend from the base of RS2 through the N-DRC base plate to the RS3, and stabilizes RS2 and RS3 on the DMTs (Bicka et al., 2022; Dymek et al., 2011; Gui et al., 2021). CFAP57 also extends through the N-DRC and interacts with RS3 via its C-terminal region (Ghanaeian et al., 2023). Recent analysis reveals that CCDC96 and CCDC113 could form a complex and extend parallel to the N-DRC and connect the base of RS3 to the tail of dynein g (IDA g) and the N-DRC (Bazan et al., 2021; Ghanaeian et al., 2023). However, the functions of these proteins in

sperm flagellum stabilization remain unknown.

Sperm flagellum is tightly anchored to the sperm head through the HTCA, a complex structure based on the centrosome (Wu et al., 2020). This structure consists of two cylindrical microtubule-based centrioles and associated components, including the well-organized segmented columns, along with the capitulum plate and basal plate. The segmented columns and capitulum plate, located below the basal plate, are thought to originate from the dense material emanating from the proximal centriole (Fawcett & Phillips, 1969; Zamboni & Stefanini, 1971). Many proteins have been identified in sperm HTCA, and their mouse models display acephalic spermatozoa syndrome phenotype (Wu et al., 2020). SPATA6 is the first protein identified as a component of the HTCA using the knockout mouse model, and is crucial for the formation of the sperm HTCA (Yuan et al., 2015). Deficiencies in SUN5 (Elkhatib et al., 2017; Fang et al., 2018; Liu et al., 2020; Sha et al., 2018; Shang et al., 2018; Shang et al., 2017; Xiang et al., 2022; Zhang et al., 2021; Zhu et al., 2016) and PMFBP1 (Deng et al., 2022; Liu et al., 2020; Liu et al., 2021; Lu et al., 2021; Nie et al., 2022; Sha et al., 2019; Zhu et al., 2018) have been demonstrated to be associated with ASS in both humans and mice. The centriole-related protein, CENTLEIN, serves as a bona fide linker between SUN5 and PMFBP1 to participates in the HTCA assembly (Zhang et al., 2021). Notably, impaired HTCA often accompanies defects in the sperm flagellum (Hall et al., 2013; Shang et al., 2017; Yuan et al., 2015; Zhang et al., 2021; Zhu et al., 2018), suggesting that the HTCA stabilization may be closely associated with the integrity of sperm flagellum. However, the mechanism that maintains both sperm flagellum and HTCA stabilization remains to be clarified.

Here, we identified an evolutionarily conserved coiled-coil domain-containing (CCDC) protein, CCDC113, and found it could complex with CFAP57 and CFAP91 for the connection of RS, N-DRC and DMTs in axoneme. The knockout of *Ccdc113* produced spermatozoa with flagella defects and head-tail linkage detachment, in turn, which caused male infertility. Ultra-structural analyses showed that the depletion of CCDC113 resulted in

the destroyed sperm axoneme and HTCA. CCDC113 is localized on the manchette, HTCA and flagellum in elongating and elongated spermatids. Further analysis revealed that CCDC113 is indispensable for the connection of CFAP91 and DRC2 to the DMTs in the sperm axoneme, and CCDC113 interacts with SUN5 and CENTLEIN to stabilize sperm HTCA. All these results suggest that CCDC113 server as a critical hub to maintain the structural integrity of both sperm flagellum and HTCA.

Results

CCDC113 complexes with CFAP57 and CFAP91 for the connection of RS, N-DRC and DMTs

CCDC113 is an evolutionarily conserved coiled-coil domain-containing (CCDC) protein in the ciliated species, and a comparative analysis of the structures of CCDC113 from *Tetrahymena thermophila* to *Homo sapiens* showed that CCDC113 orthologs shared structural similarity with each other (Fig. 1A). Recent cryo-EM analysis in the structure of the 96-nm modular repeats of axonemes from the *Tetrahymena thermophila* cilia and human respiratory cilia revealed that CCDC113 localized the linker region among RS, N-DRC and DMTs (Fig. 1B), indicating it may serve as a structural component connecting RS, N-DRC and DMTs (Bazan et al., 2021; Ghanaeian et al., 2023). To investigate further, we examined the interactions between CCDC113 and its neighboring axoneme-associated proteins, CFAP57 and CFAP91 (Fig. 1B). We transfected HEK293T cells with a GFP-tagged CCDC113 and FLAG-tagged CFAP57 or CFAP91, and then performed anti-FLAG-immunoprecipitations (Fig. 1A). CCDC113 were present in both FLAG-CFAP57 and FLAG-CFAP91 immunoprecipitates (Fig. 1C, D), indicating CCDC113 interacts with both CFAP57 and CFAP91. Given that CFAP91 have been reported to stabilize RS on the DMTs (Bicka et al., 2022; Dymek et al., 2011; Gui et al., 2021) and the cryo-EM analysis shows CCDC113 is closed to DMTs, we speculate CCDC113 may connect RS to DMTs via binding CFAP91 and microtubules. To test it, we detected the interaction between CCDC113 and β-tubulin (TUBB5), and found CCDC113 was present in MYC-TUBB5 immunoprecipitate (Fig. 1E). As CFAP57 extends through the N-DRC and CCDC113 is closed to the N-DRC (Ghanaeian

et al., 2023), we further examined the interaction between CCDC113 and N-DRC components that closed to DMTs. The co-immunoprecipitation (co-IP) analysis showed that CCDC113 could bind to DRC1, DRC2, and DRC3 (Fig. 1E-H). Therefore, CCDC113 may be serve as an adaptor protein for the connection of RS, N-DRC and DMTs, and this protein may be a critical hub for axoneme stabilization.

CCDC113 is required for male fertility

To investigate the physiological functions of CCDC113, we generated a *Ccdc113* knockout mouse strain using the CRISPR/Cas9 system (Fig. 2A). *Ccdc113*$^{-/-}$ mice were genotyped by genomic DNA sequencing and further confirmed by polymerase chain reaction (PCR). Genotypes were distinguished by a 539 bp band for *Ccdc113*$^{+/+}$ mice, a 461 bp band for *Ccdc113*$^{-/-}$ mice, and two bands of 539 bp and 461 bp for *Ccdc113*$^{+/-}$ mice (Fig. 2B). Further immunoblotting analysis validated the successful elimination of CCDC113 in total protein extracts from *Ccdc113*$^{-/-}$ testes (Fig. 2C). Mice lacking *Ccdc113* showed no gross abnormalities in appearance or behavior, and no obvious differences in body weight (Fig. 2H). Symptoms such as hydrocephalus or left-right asymmetry defects were also not found in *Ccdc113*$^{-/-}$ mice (Fig. S1A). Additionally, the deficiency of CCDC113 did not affect ciliogenesis in the lung and trachea (Fig. S1B-D). Subsequently, we assessed the fertility of 2-month-old male and female *Ccdc113*$^{-/-}$ mice. *Ccdc113*$^{-/-}$ female mice were able to generate offspring after mating with wild-type (WT) adult males, which was similar to *Ccdc113*$^{+/+}$ female mice (Fig. 2D). However, *Ccdc113*$^{-/-}$ male mice exhibited normal mating behavior with copulatory plugs but failed to produce any offspring after mating with WT adult female mice (Fig. 2E). Thus, the knockout of *Ccdc113* results in male infertility.

***Ccdc113* knockout mice produce spermatozoa with flagella defects and head-tail linkage detachment**

To further investigate the cause of male infertility, we initially examined *Ccdc113*$^{-/-}$ testis at both gross and histological levels. *Ccdc113* knockout did not affect either testis size (Fig. 2F, G) or the ratio of testis weight to body weight (Fig. 2H, I). Histological sections stained with

hematoxylin-eosin (H&E) revealed that seminiferous tubules of *Ccdc113*$^{+/+}$ mice exhibited a tubular lumen with flagella emerging from the developing spermatids. In contrast, the flagellum staining appeared reduced in *Ccdc113*$^{-/-}$ seminiferous tubules (Fig. 2J, red asterisk). Immunofluorescence staining for acetylated tubulin (ac-tubulin), a marker for sperm flagellum (Martinez et al., 2020), further confirmed the defects of flagellum in *Ccdc113*$^{-/-}$ mice (Fig. 2K). Next, we examined spermatids at different stages in *Ccdc113*$^{-/-}$ testes by using Periodic acid–Schiff (PAS) staining, and found that the acrosome biogenesis and nucleus morphology in *Ccdc113*$^{-/-}$ spermatids from step 1 to step 10 were normal compared to *Ccdc113*$^{+/+}$ spermatids. However, abnormal club-shaped heads were observed in *Ccdc113*$^{-/-}$ spermatids from step 11 to step 16 (Fig. S2A, black asterisk). In addition, the manchette of *Ccdc113*$^{-/-}$ spermatids were more elongated compared to that of *Ccdc113*$^{+/+}$ spermatids (Fig. S2B). Therefore, the disruption of CCDC113 impaired spermiogenesis.

Next, we examined the spermatozoa in the caudal epididymis, and found that the sperm count in the *Ccdc113*$^{-/-}$ caudal epididymis was significantly decreased compared with the control group (Fig. 3A, B). The motility of the released spermatozoa from *Ccdc113*$^{+/+}$ and *Ccdc113*$^{-/-}$ cauda epididymis showed that the *Ccdc113*$^{-/-}$ spermatozoa were completely immobility (Fig. 3C). H&E staining of the caudal epididymis showed fewer hematoxylin-stained sperm heads in the *Ccdc113*$^{-/-}$ cauda epididymis compared to that of the *Ccdc113*$^{+/+}$ cauda epididymis. Notably, in contrast to the control group, where the epididymal lumen exhibited linear eosin staining, the *Ccdc113*$^{-/-}$ mouse showed a dramatic presence of coiled eosin-stained structures without sperm heads in the epididymal lumen (Fig. 3A, red circles). To determine the morphological characteristics of the spermatozoa, we conducted single-sperm immunofluorescence using an anti-α/β-tubulin antibody to label the sperm flagellum and lectin peanut agglutinin (PNA) to visualize the sperm acrosome (Nakata et al., 2015). We noticed that *Ccdc113*$^{-/-}$ spermatozoa showed severe morphological malformations, including sperm head-tail detachment (type 1), abnormal sperm head with curly tail (type 2), normal sperm head with curly tail (type 3) (Fig. 3D, E). Overall, these findings clearly suggest that the deletion of *Ccdc113* results in both sperm flagellum deformity and detachment of sperm

head-to-tail linkage, and causes a special type of acephalic spermatozoa, which may be responsible for the *Ccdc113*$^{-/-}$ male infertility.

CCDC113 localizes on the sperm neck and flagellum regions

To gain further insights into the functional role of CCDC113 during spermiogenesis, we detected the expression of CCDC113, and found that CCDC113 was predominantly expressed in mouse testis (Fig. 4A). Furthermore, CCDC113 was first detected in testis at postnatal day 7 (P7), and the level of CCDC113 increased continuously from P21 onward, with the highest levels detected in adult testes (Fig. 4B), indicating CCDC113 might be highly expressed during spermiogenesis. Then, we conducted immunofluorescence analysis of CCDC113 in *Ccdc113*$^{+/+}$ and *Ccdc113*$^{-/-}$ germ cells to characterize its precise localization during spermatogenesis (Fig. S3). CCDC113 showed punctum single near the nuclei of spermatocyte and round spermatids, and localized on the manchette, sperm neck and flagellum regions in elongating and elongated spermatids (Fig. S3).

To further confirm it, we co-stained CCDC113 and α/β-tubulin, which represented the manchette and flagellum in spermatids (Lehti & Sironen, 2016) (Fig. 4D). The immunofluorescence analysis showed that CCDC113 localized on the manchette surrounding the spermatid head from step 9 to step 14, as well as the testicular sperm neck and flagellum (Fig. 4D). Given that CCDC113 was initially identified as a component of centriolar satellites (Firat-Karalar et al., 2014), the punctum single of CCDC113 in spermatocyte and spermatids may localize around the centrosome. To test it, we performed the immunofluorescent staining of CCDC113 and centrosomal protein CENTRIN1/2 in spermatocytes and spermatids, and found the signal of CCDC113 could partially colocalize with CENTRIN1/2 (Fig. 4C). Thus, CCDC113 localizes on the centrosome, manchette, sperm neck and flagellum regions in the developing germ cells.

Next, we examined the localization of CCDC113 in mature spermatozoa, and found that CCDC113 was localized in the sperm neck and flagellum regions (Fig. 4E). Similar localization of CCDC113 could also be detected in human mature spermatozoa (Fig. 4F).

Therefore, the localization of CCDC113 on the sperm neck and flagellum is persistent in mature spermatozoa, which may be essential for the integrity of sperm flagellum and head to tail.

Ccdc113 **knockout results in the disorganization of the sperm flagellum structures**

To delineate the sperm flagella defects in *Ccdc113*$^{-/-}$ mice, we conducted transmission electron microscopy (TEM) examination of longitudinal sections of *Ccdc113*$^{-/-}$ spermatozoa. The TEM analysis revealed a significant presence of unremoved cytoplasm, including disrupted mitochondria, damaged axonemes, and large vacuoles in *Ccdc113*$^{-/-}$ spermatozoa (Fig. 5A, red asterisks). Cross sections of the principal piece of *Ccdc113*$^{-/-}$ spermatozoa further revealed partial loss or unidentifiable "9+2" axonemal structures, along with the disruption of the fibrous sheath and outer dense fibers (Fig. 5A). We further examined the axonemal structure in *Ccdc113*$^{-/-}$ testicular spermatids using TEM, and disorganized axonemal microtubules were detected in *Ccdc113*$^{-/-}$ testicular spermatids (Fig. 5B). In contrast to the regular positioning of the CP and nine peripheral DMTs in the *Ccdc113*$^{+/+}$ spermatid axoneme, the *Ccdc113*$^{-/-}$ spermatids exhibited a scattered arrangement of DMTs, and no distinct radial spokes were observed (Fig. 5B, red arrowheads). Diffused axonemal signals could also be observed in *Ccdc113*$^{-/-}$ testicular germ cells by using ac-tubulin immunofluorescence staining during spermiogenesis (Fig. 5B, Fig. S2C). These results indicated CCDC113 is essential for the integrity of sperm flagellum.

CCDC113 has been shown to localize at the base of the RS3 and interact with neighboring axoneme-associated proteins (Fig. 1B-H). Since obvious disorganized “9+2” axonemal structure was detected in the cross-sectioned *Ccdc113*$^{-/-}$ flagellar specimen (Fig. 5A, B), we speculated that CCDC113 likely served as an adaptor to connect the neighboring axoneme-associated proteins to DMTs. Pursuing this, we examined the flagellar localization of CFAP91 in *Ccdc113*$^{-/-}$ spermatozoa, which is positioned in close proximity to CCDC113 at the root region of RS3, critical for the localizations of calmodulin-associated and spoke-associated complex (CSC) proteins CFAP61 and CFAP251 (Bicka et al., 2022; Meng et al., 2024).

Immunofluorescence results indicated that the absence of *Ccdc113* leads to the abnormal distribution of CFAP91 on the axoneme, where CFAP91 could not colocalize with DMTs. (Fig. 5C, white asterisks and 5E). Given that DRC2 serves as the core component of the axonemal N-DRC (Jreijiri et al., 2023) and CCDC113 could bind to DRC2 (Fig 1G), we further detected DRC2 localization in the *Ccdc113*$^{+/+}$ and *Ccdc113*$^{-/-}$ spermatozoa. Immunofluorescence analysis showed that DRC2 exhibited distinct signals that were not colocalized with DMTs of *Ccdc113*$^{-/-}$ spermatozoa (Fig. 5D, white asterisks and 5F). These findings collectively indicate that CCDC113 is indispensable for the connection of CFAP91 and DRC2 to the DMTs, which is required for structural integrity of the sperm axoneme.

***Ccdc113* knockout impairs head-to-tail anchorage of the spermatids**

To address how *Ccdc113* knockout caused acephalic spermatozoa, we initially examined wherein the flagellum detached from sperm head in *Ccdc113*$^{-/-}$ mice. The proportion of decapitated tails in the *Ccdc113*$^{-/-}$ caput, corpus and caudal of the epididymis exhibited similar proportions (Fig. 6A), indicating the separation of the sperm head and tail in *Ccdc113*$^{-/-}$ mice may occur either within the seminiferous tubules or upon entering the caput of the epididymis. To confirm it, we performed PAS staining to examine the stages of spermiogenesis in *Ccdc113*$^{+/+}$ and *Ccdc113*$^{-/-}$ testes (Fig. 6B). We found that *Ccdc113*$^{+/+}$ sperm heads in stages VII-VIII were oriented towards the basal membrane, whereas *Ccdc113*$^{-/-}$ sperm heads were oriented towards the tubule lumen during stages VII-VIII (Fig. 6C, arrows), which may be attributed to the separation of sperm heads from flagellum during spermiogenesis. Additionally, mature sperm heads were still observable at stages IX–X in *Ccdc113*$^{-/-}$ testes, while mature spermatozoa were released into the lumen of the seminiferous tubule at stage VIII in *Ccdc113*$^{+/+}$ testes (Fig. 6B, red asterisk). These results suggest that the sperm head and flagellum might undergo separation during spermiation in the *Ccdc113*$^{-/-}$ testes.

Next, we examined the development of the HTCA in *Ccdc113*$^{+/+}$ and *Ccdc113*$^{-/-}$ spermatids using TEM. In *Ccdc113*$^{+/+}$ step 9–11 spermatids, the well-defined coupling apparatus

consisted of basal plate, capitulum plate, segmented columns, proximal centriole, distal centriole was tightly attached to the sperm head. However, in *Ccdc113*$^{-/-}$ step 9–11 spermatids, the abnormal HTCA detached from the sperm head (Fig.6D, red asterisk). Further observation of the HTCA structure revealed the absence of segmented columns and capitulum plate; only dense material surrounding the proximal centriole and basal plate could be detected (Fig. 6D, white arrow). The basal plates were abnormally distant from their native implantation site on the nucleus of *Ccdc113*$^{-/-}$ elongating and elongated spermatids (Fig. 6D). Taken together, our results indicate that the disruption of *Ccdc113* causes the destroyed coupling apparatus detachment from the sperm head during spermiogenesis, and CCDC113 is required for the integrity of the sperm HTCA.

CCDC113 cooperates with SUN5 and CENTLEIN to stabilize sperm HTCA

To investigate the molecular function of CCDC113 in sperm head-tail linkage, we examined interaction between CCDC113 and reported HTCA-associated proteins, including SUN5, CENTLEIN, PMFBP1, and SPATA6 (Shang et al., 2017; Yuan et al., 2015; Zhang et al., 2021; Zhu et al., 2018). GFP-tagged CCDC113 and FLAG-tagged HTCA-associated proteins were co-transfected into HEK293T cells, followed by the immunoprecipitation with anti-GFP antibody. We found that CCDC113 could interact with SUN5 and CENTLEIN, but not with PMFBP1 and SPATA6 (Fig. 7A-C, F). We further conducted co-immunoprecipitation assays in the reverse direction and verified that both SUN5 and CENTLEIN could bind to CCDC113 (Fig. 7D, E). To further investigate the localization of CCDC113 in the HTCA, we co-stained mature spermatozoa with antibodies against CCDC113 and SUN5, which has been reported to be localized on the root connecting the HTCA to the nuclear envelope (Shang et al., 2017; Zhang et al., 2021). CCDC113 was located below SUN5, showed partial overlap with SUN5 (Fig. 7G). The centriolar protein CENTLEIN was detected to localize on the HTCA and acted as the critical linker protein between SUN5 and PMFBP1 in the elongating and elongated spermatid (Zhang et al., 2021)). Given that CENTLEIN disappears in mature spermatozoa (Zhang et al., 2021), we performed the immunofluorescent staining of CCDC113 and CENTLEIN in elongated spermatids, and found that CCDC113 could partially colocalize with

CENTLEIN at the HTCA (Fig. 7H). Thus, CCDC113 could interact with both SUN5 and CENTLEIN, and localize on the sperm HTCA.

The HTCA localization of CCDC113 may be response for the integrity of HTCA. To test it, we detected the localization of classical HTCA component, SPATA6, in *Ccdc113*$^{-/-}$and *Ccdc113*$^{+/+}$spermatozoa by performing the immunofluorescent staining. We found that SPATA6 was not attached to the implantation fossa of the sperm nucleus (Fig. 7I, J), indicating that CCDC113 is essential for the integrity of sperm HTCA. To further understand the functional relationships among CCDC113, SUN5, and CENTLEIN at the sperm HTCA, we examined the localization of CCDC113 in *Sun5*$^{-/-}$ and *Centlein*$^{-/-}$ spermatozoa. Compared to the control group, CCDC113 predominantly localized on the decapitated flagellum in both *Sun5*$^{-/-}$ and *Centlein*$^{-/-}$ spermatozoa (Fig. 7K, L), indicating SUN5 and CENTLEIN are indispensable for the docking of CCDC113 to the implantation site on the sperm head. Taken together, these data demonstrate that CCDC113 cooperate with SUN5 and CENTLEIN to stabilize sperm HTCA and anchor the sperm head to the tail.

Discussion

CCDC113 is a highly evolutionarily-conserved component of motile cilia/flagella. Studies in the model organism *Tetrahymena thermophila* have revealed that CCDC113 connects RS3 to dynein g and the N-DRC, which plays essential role in cilia motility (Bazan et al., 2021; Ghanaeian et al., 2023). However, the physiological functions of CCDC113 in mammals remain unknown. In this study, we reveal that CCDC113 is indispensable for male fertility, as *Ccdc113* knockout mice produce spermatozoa with flagella defects and head-tail linkage detachment (Fig. 3D). CCDC113 is localized on the sperm neck and flagellum regions in the elongating and elongated spermatids. In sperm flagellum, CCDC113 could interact with both CFAP57 and CFAP91, and serve as an adaptor protein for the connection of RS, N-DRC and DMTs to stabilize sperm flagellum. In sperm head to tail connecting piece, CCDC113 could bind to SUN5 and CENTLEIN to stabilize sperm HTCA and anchor the sperm head to the tail. Thus, CCDC113 is essential for the integrity of both sperm axoneme and sperm HTCA.

Recent cryo-EM analysis in the axonemes from *Tetrahymena thermophila* cilia and human respiratory cilia revealed that CCDC113 localized the linker region among RS3, N-DRC and DMTs (Bazan et al., 2021; Ghanaeian et al., 2023), and we found that CCDC113 indeed interacted with its neighboring axoneme-associated proteins, CFAP57 and CFAP91 (Fig. 1C, D). CFAP57 has been identified as the adaptor protein responsible for assembling dynein g and d, and it can interact with both N-DRC and RS3 (Ghanaeian et al., 2023; Ma et al., 2023). Previous studies demonstrated that CFAP91 extended from the base of RS2 through the N-DRC base plate to RS3, playing a crucial role in stabilizing and localizing RS2 and RS3 on the DMT (Bicka et al., 2022; Dymek et al., 2011; Gui et al., 2021). The CFAP91 ortholog, FAP91, interacts with three N-DRC subunits (DRC1, DRC2, and DRC4), participating in the docking of the N-DRC in *Chlamydomonas* (Gui et al., 2021). In humans, pathogenic mutations in CFAP91 and DRC2 disrupt sperm flagellum structure, result in MMAF (Jreijiri et al., 2023; Martinez et al., 2020). TEM and immunostaining experiments in spermatozoa showed severe CP and radial spokes defects in *CFAP91* mutant patients (Martinez et al., 2020). In this study, we found that the absence of CCDC113 results in severe axonemal disorganization characterized by defective RSs, scattered DMTs, and misplaced CP. Further analysis demonstrated that the deficiency of CCDC113 disrupts the localization of CFAP91 and DRC2 on DMTs. Thus, CCDC113 may function as an adaptor protein to stabilize CFAP91 and DRC2 on the DMT, which facilitates the docking of RS and N-DRC to DMTs, thereby maintaining the integrity of sperm axoneme.

Recent analysis has revealed that certain centrosomal proteins play crucial roles in the assembly and maintenance of sperm HTCA (Avasthi et al., 2013; Liska et al., 2009; Zhang et al., 2021). In early round spermatids, the centriole pair initially localizes to the caudal nuclear pole and expands the electron-dense material, part of which shows striation (Wu et al., 2020). Along with the development of spermatids, the dense material around the centrioles gradually transforms into a well-organized structure, clearly identified as basal plate, capitulum plate and segmented columns (Dooher & Bennett, 1973; Wu et al., 2020). CCDC113 was initially

identified through the isolation of centriolar proteins from bovine sperm (Firat-Karalar et al., 2014). During spermiogenesis, CCDC113 could colocalize with CENTRIN1/2 at the centrosome in developing spermatids, and continue to localize on the sperm neck region in elongating and elongated spermatids (Fig. 4C, D). In addition, CCDC113 could bind to HTCA associated centrosomal protein, CENTLEIN, and the disruption of *Centlein* impaired the attachment of CCDC113 to sperm head. In the *Ccdc113*$^{-/-}$spermatids, the capitulum plate and segmented columns were absent, and the basal plate were detached from the implantation site on the nucleus of *Ccdc113*$^{-/-}$ elongating and elongated spermatids during spermiogenesis (Fig. 6D). These observations raise the possibility that CCDC113 might be a HTCA associated centrosomal protein, and play a role in maintaining the structural integrity of the HTCA.

SUN5 is a transmembrane protein located in the nuclear envelope, and acts as the root that connects the HTCA to the sperm nuclear envelope (Shang et al., 2017). CENTLEIN could directly bind to SUN5 and PMFBP1, and works as a linker between SUN5 and PMFBP1 to maintain the integrity of HTCA (Zhang et al., 2021). CCDC113 could interact with SUN5 and CENTLEIN, but not PMFBP1 (Fig. 7A-C), and CCDC113 was in the cytoplasm in *Sun5*$^{-/-}$ and *Centlein*$^{-/-}$ spermatozoa (Fig. 7L, K). In addition, CCDC113 colocalizes with SUN5 in the HTCA region, and the immunofluorescence staining in spermatozoa shows that SUN5 is closer to the sperm nucleus than CCDC113 (Fig. 7G, H). Therefore, SUN5 and CENTLEIN may be more closed to the sperm nucleus compared with CCDC113.

Overall, we identified CCDC113 as a structural component of both the flagellar axoneme and the HTCA, playing dual roles in stabilizing the sperm axonemal structure and maintaining the structural integrity of HTCA. As *Ccdc113*$^{-/-}$ mice did not exhibit other ciliopathies, such as situs inversus, hydrocephalus, and abnormal ciliogenesis of tracheal cilia (Fig. S1A-D), indicating CCDC113 may specially function in spermiogenesis. Given the evolutionary conservation of CCDC113 in humans, we speculate that mutations in *CCDC113* may be present in individuals with MMAF or ASS. Men with sperm flagella defects and head-tail linkage detachment may be a new type of ASS.

Materials and Methods

Phylogenetic analysis and structural similarity analysis

Amino acid sequence of CCDC113 of 7 species were downloaded from UniProt. The phylogenetic trees were constructed using MEGA 10.0 (Kumar et al., 2018) with the Neighbor-Joining (NJ) method (Saitou & Nei, 1987). 3D structures of CCDC113 orthologs of 7 species were obtained from AlphaFold Protein Structure Database (Varadi et al., 2022). Structural similarity Z scores were derived through the DALI webserver for all against all structure comparison (Holm & Laakso, 2016).

Animals

The mouse *Ccdc113* gene is 44.81 kb and contains 9 exons. Exon 2 to exon 6 of *Ccdc113* was chosen as the target site. The knockout mice were generated by CRISPR-Cas9 system from Cyagen Biosciences. The gRNA and Cas9 mRNA were co-injected into fertilized eggs of C57BL/6J mice to generate *Ccdc113*$^{+/-}$ mice with a 10215 bp base deletion and 64 bp insertion. The resulting heterozygotes were interbred to obtain offspring, which further were genotyped by genomic DNA sequencing to obtain widetype and homozygote mice. The genotyping primers for knockout were: F1: 5'-TCAAATCATCACACCCTGCCTCT-3', R: 5'-GCTTGCACTCGGGTGATACATAA-3', and for WT mice, the specific primers were: F2: 5'-CAGGTTCTCAACACCTACAAAGTA-3', R: 5'-GCTTGCACTCGGGTGATACATAA-3'.

All the animal experiments were performed according to approved institutional animal care and use committee (IACUC) protocols (# 08-133) of the Institute of Zoology, Chinese Academy of Sciences.

Human adult sperm sample preparation

The sperm donation candidates in this study were healthy young Chinese men. Each participant underwent a thorough medical examination and completed an extensive medical and social questionnaire to ensure the exclusion of individuals with genetic or significant medical issues, as outlined in the Basic Standard and Technical Norms of Human Sperm Bank published by the Chinese Ministry of Health. Individuals who smoked, abused drugs, or were

423 heavy drinkers were also excluded from the study. Those who remained eligible signed
424 informed consent forms for voluntary sperm donation and agreed to reside in Beijing for a
425 minimum of six months. The sperm bank documented each participant's age, date of birth,
426 and date of semen collection. Ethical approval for this study was granted by the Reproductive
427 Study Ethics Committee of Peking University Third Hospital (2017SZ-035). Semen samples
428 were processed using a 40% density gradient of PureSperm (Nidacon International, Molndal,
429 Sweden) through centrifugation at room temperature (500 × g, 30 min) and washed three
430 times with phosphate-buffered saline (PBS). The obtained spermatozoa were utilized for
431 immunofluorescence staining.

432 **Antibodies**

433 Rabbit anti-CCDC113 generated from Dia-an Biotech (Wuhan, China) was diluted at 1:500
434 for western blotting and a 1: 25 dilution for immunofluorescence. Mouse anti-α-TUBULIN
435 antibody (AC012, Abclonal) was used at a 1:5000 dilution for western blotting. Mouse anti-
436 GFP antibody (M20004, Abmart) was used at a 1:2000 dilution for western blotting. Rabbit
437 anti-MYC antibody (BE2011, EASYBIO) was used at a 1:2000 dilution for western blotting.
438 Rabbit anti-FLAG antibody (20543-1 AP, Proteintech) was used at a 1:2000 dilution for
439 western blotting. Mouse anti-ac-TUBULIN antibody (T7451, Sigma-Aldrich) was used at a
440 1:200 dilution for immunofluorescence. Mouse anti-α/β-TUBULIN antibody (ab44928,
441 Abcam) was used at a 1: 100 dilution for immunofluorescence. Rabbit anti-DRC2 antibody
442 (NBP2-84617, Novus) was used at a 1:100 dilution for immunofluorescence. Rabbit anti-
443 CFAP91 antibody (bs-9823R, Bioss) was used at a 1:100 dilution for immunofluorescence.
444 In-house-generated mouse anti-SUN5 antibody targeting the SUN5 SUN domain (aa193–373)
445 was used at a 1:100 dilution for immunofluorescence analysis. Rat anti-CENTLEIN antibody
446 was generated by Absea Biotechnology Ltd (Beijing, China) was diluted at a 1:20 dilution for
447 immunofluorescence. Rabbit anti-SPATA6 antibody (11849 -1 AP, Proteintech) was used at a
448 1:100 dilution for immunofluorescence. The Alexa Fluor 488 conjugate of lectin PNA (1:400,
449 L21409, Thermo Fisher) was used for immunofluorescence. The secondary antibodies were
450 goat anti-rabbit FITC (1:200, ZF-0311, Zhong Shan Jin Qiao), goat anti-rabbit TRITC (1:200,
451 ZF-0316, Zhong Shan Jin Qiao), goat anti-mouse FITC (1:200, ZF-0312, Zhong Shan Jin

Qiao) and goat anti-mouse TRITC (1:200, ZF0313, Zhong Shan Jin Qiao).

Sperm motility and sperm count assays

The cauda epididymis was isolated from 8 weeks of mice. Sperm were released in phosphate-buffered saline (PBS, Gibco, C14190500BT) from the incisions of the cauda epididymis for 10 min at 37 ℃. And then the swim-up suspension was used for the analysis of sperm motility with a microscope through a 20x phase objective. Viewing areas in each chamber were imaged using a CCD camera. The samples were analyzed via computer-assisted semen analysis (CASA) using the Minitube Sperm Vision Digital Semen Evaluation System (12500/1300, Minitube Group, Tiefenbach, Germany) and were also analyzed by a computer-aided semen analysis system (CASA). The incubated sperm number was counted with a hemocytometer.

Histology staining

As previously reported (Wang et al., 2018), the testes and caudal epididymis were dissected after euthanasia, and fixed with Bouin's fixative for 24 h at 4 ℃, then the testes were dehydrated with graded ethanol and embedded in paraffin. For histological analysis, the 5 μm sections were cut and covered on glass slides. Sections were stained with H&E and PAS for histological analysis after deparaffinization.

Electron microscopy analysis

The cauda epididymis and testis were dissected and fixed in 2.5% (vol/vol) glutaraldehyde in 0.1 M cacodylate buffer at 4℃ overnight. After washing in 0.1 M cacodylate buffer, samples were cut into small pieces of approximately 1 mm^3, then immersed in 1% OsO4 for 1 h at 4℃. Samples were dehydrated through a graded acetone series (50%, 60%, 70%, 80%, 90%, 95%, 100%) and embedded in resin (DDSA, NMA, enhancer, 812) for staining. Ultrathin sections were cut and stained with uranyl acetate and lead citrate. Images were acquired and analyzed using a JEM-1400 transmission electron microscope.

Scanning electron microscopy

The trachea was fixed in 2.5% glutaraldehyde solution overnight, and dehydrated in graded ethanol, subjected to drying and coated with gold. The images were acquired and analyzed using SU8010 scanning electron microscope.

481 **Immunofluorescence staining**

482 The testis albuginea was peeled and incubated with collagenase IV and hyaluronidase in PBS
483 for 15 min at 37℃, then washed twice with PBS. Next, fixed with 4% PFA for 5 min, and
484 then coated on slide glass to dry out. The slides were washed with PBS three times and then
485 treated with 0.5% TritonX-100 for 5 min, and blocked with 5% BSA for 30 min. Added the
486 primary antibodies and incubated at 4℃ overnight, followed by incubating with a second
487 antibody and DAPI. The images were taken using LSM880 and SP8 microscopes.

488

489 The mouse testis was immediately dissected and fixed with 2% paraformaldehyde in 0.05%
490 PBST (PBS with 0.05% Triton X-100) at room temperature for 5 min. The fixed sample was
491 placed on a slide glass and squashed by placing a cover slip on top and pressing down. The
492 sample was immediately flash frozen in liquid nitrogen, and the slides were stored at −80°C
493 for further immunofluorescence experiments. After removing the coverslips, the slides were
494 washed with PBS three times and then treated with 0.1% Triton X-100 for 10 min, rinsed
495 three times in PBS, and blocked with 5% bovine serum albumin (Amresco, AP0027). The
496 primary antibody was added to the sections and incubated at 4°C overnight, followed by
497 incubation with the secondary antibody. The nuclei were stained with DAPI. The
498 immunofluorescence images were taken immediately using an LSM 780 microscope (Zeiss)
499 or SP8 microscope (Leica).

500

501 Spermatozoa were released from the cauda epididymis in PBS at 37°C for 15 min, then were
502 spread on glass slides for morphological observation or immunostaining. After air drying,
503 spermatozoa were fixed in 4% PFA for 5 min at room temperature, and slides were washed
504 with PBS three times and blocked with 5% BSA for 30 min at room temperature. The primary
505 antibodies were added to the sections and incubated at 4°C overnight, followed by incubation
506 with the secondary antibody. The nuclei were stained with DAPI and images were taken using
507 an LSM 880 microscope (Zeiss) or SP8 microscope (Leica).

508 **Immunoprecipitation**

509 Transfected cells were lysed in a lysis buffer (50mM HEPES, PH 7.4, 250mM NaCl, 0.1%

NP-40 containing PIC and PMSF) on ice for 30 min and centrifugated at 12000 rpm at 4°C for 15 min, cell lysates were incubated with primary antibody about 12 hours at 4°C and then incubated with protein A-Sepharose (GE, 17-1279-03) for 3 hours at 4°C, then washed three times with lysed buffer and subjected to immunoblotting analysis.

Statistical analysis

All the experiments were repeated at least three times, and the results are presented as the mean ± SD. The statistical significance of the differences between the mean values for the different genotypes was measured by the Student's t-test with a paired, 2-tailed distribution. The data were considered significant when the *P*-value was less than 0.05(*), 0.01(**), 0.001(***) or 0.0001(****).

Acknowledgements

This work was supported by the National Science Fund for Distinguished Young Scholars (Grant No. 81925015), National Natural Science Foundation of China (Grant No. 32230029, 82371615) and National Key Research and Development Program of China (Grant No. 2022YFC2702600).

Author Contributions

B.W. and C.L. performed most of the experiments and wrote the manuscript. Y.Y., Z.Z., and H.J. provided human adult sperm sample and performed some of the immunofluorescence experiments. S.M., Y.M., H.W., and J.L. contributed to the cell experiments and animal breeding. W.L. and C.L. supervised the whole project and revised the manuscript.

Declaration of interests

The authors declare that they have no conflict of interest.

References

Avasthi, P., Scheel, J. F., Ying, G., Frederick, J. M., Baehr, W., & Wolfrum, U. (2013). Germline deletion of Cetn1 causes infertility in male mice. *J Cell Sci*, *126*(Pt 14), 3204-3213. https://doi.org/10.1242/jcs.128587

Bazan, R., Schröfel, A., Joachimiak, E., Poprzeczko, M., Pigino, G., & Wloga, D. (2021). Ccdc113/Ccdc96 complex, a novel regulator of ciliary beating that connects radial

539 spoke 3 to dynein g and the nexin link. *PLoS Genet*, *17*(3), e1009388.
540 https://doi.org/10.1371/journal.pgen.1009388
541 Bicka, M., Joachimiak, E., Urbanska, P., Osinka, A., Konopka, A., Bulska, E., & Wloga, D.
542 (2022). Cfap91-Dependent Stability of the RS2 and RS3 Base Proteins and Adjacent
543 Inner Dynein Arms in Tetrahymena Cilia. *Cells*, *11*(24), 4048.
544 https://doi.org/10.3390/cells11244048
545 Canty, J. T., Tan, R., Kusakci, E., Fernandes, J., & Yildiz, A. (2021). Structure and Mechanics
546 of Dynein Motors. *Annu Rev Biophys*, *50*, 549-574. https://doi.org/10.1146/annurev-
547 biophys-111020-101511
548 Deng, T. Q., Xie, Y. L., Pu, J. B., Xuan, J., & Li, X. M. (2022). Compound heterozygous
549 mutations in PMFBP1 cause acephalic spermatozoa syndrome: A case report. *World J*
550 *Clin Cases*, *10*(34), 12761-12767. https://doi.org/10.12998/wjcc.v10.i34.12761
551 Dooher, G. B., & Bennett, D. (1973). Fine structural observations on the development of the
552 sperm head in the mouse. *Am J Anat*, *136*(3), 339-361.
553 https://doi.org/10.1002/aja.1001360307
554 Dymek, E. E., Heuser, T., Nicastro, D., & Smith, E. F. (2011). The CSC is required for
555 complete radial spoke assembly and wild-type ciliary motility. *Mol Biol Cell*, *22*(14),
556 2520-2531. https://doi.org/10.1091/mbc.E11-03-0271
557 Elkhatib, R. A., Paci, M., Longepied, G., Saias-Magnan, J., Courbiere, B., Guichaoua, M. R.,
558 Levy, N., Metzler-Guillemain, C., & Mitchell, M. J. (2017). Homozygous deletion of
559 SUN5 in three men with decapitated spermatozoa. *Human Molecular Genetics*,
560 *26*(16), 3167-3171. https://doi.org/10.1093/hmg/ddx200
561 Fang, J., Zhang, J., Zhu, F., Yang, X., Cui, Y., & Liu, J. (2018). Patients with acephalic
562 spermatozoa syndrome linked to SUN5 mutations have a favorable pregnancy
563 outcome from ICSI. *Hum Reprod*, *33*(3), 372-377.
564 https://doi.org/10.1093/humrep/dex382
565 Fawcett, D. W., & Phillips, D. M. (1969). The fine structure and development of the neck
566 region of the mammalian spermatozoon. *Anat Rec*, *165*(2), 153-164.
567 https://doi.org/10.1002/ar.1091650204

568 Firat-Karalar, E. N., Sante, J., Elliott, S., & Stearns, T. (2014). Proteomic analysis of
569 mammalian sperm cells identifies new components of the centrosome. *J Cell Sci*,
570 *127*(Pt 19), 4128-4133. https://doi.org/10.1242/jcs.157008
571 Ghanaeian, A., Majhi, S., McCafferty, C. L., Nami, B., Black, C. S., Yang, S. K., Legal, T.,
572 Papoulas, O., Janowska, M., Valente-Paterno, M., Marcotte, E. M., Wloga, D., & Bui,
573 K. H. (2023). Integrated modeling of the Nexin-dynein regulatory complex reveals its
574 regulatory mechanism. *Nat Commun*, *14*(1), 5741. https://doi.org/10.1038/s41467-
575 023-41480-7
576 Gui, M., Ma, M., Sze-Tu, E., Wang, X., Koh, F., Zhong, E. D., Berger, B., Davis, J. H.,
577 Dutcher, S. K., Zhang, R., & Brown, A. (2021). Structures of radial spokes and
578 associated complexes important for ciliary motility. *Nat Struct Mol Biol*, *28*(1), 29-37.
579 https://doi.org/10.1038/s41594-020-00530-0
580 Hall, E. A., Keighren, M., Ford, M. J., Davey, T., Jarman, A. P., Smith, L. B., Jackson, I. J., &
581 Mill, P. (2013). Acute versus chronic loss of mammalian Azi1/Cep131 results in
582 distinct ciliary phenotypes. *PLoS Genet*, *9*(12), e1003928.
583 https://doi.org/10.1371/journal.pgen.1003928
584 Holm, L., & Laakso, L. M. (2016). Dali server update. *Nucleic Acids Res*, *44*(W1), W351-
585 355. https://doi.org/10.1093/nar/gkw357
586 Inaba, K., & Mizuno, K. (2016). Sperm dysfunction and ciliopathy. *Reprod Med Biol*, *15*(2),
587 77-94. https://doi.org/10.1007/s12522-015-0225-5
588 Ishikawa, T. (2017). Axoneme Structure from Motile Cilia. *Cold Spring Harbor Perspectives*
589 *in Biology*, *9*(1), a028076. https://doi.org/10.1101/cshperspect.a028076
590 Jreijiri, F., Cavarocchi, E., Amiri-Yekta, A., Cazin, C., Hosseini, S. H., El Khouri, E., Patrat,
591 C., Thierry-Mieg, N., Ray, P. F., Duliouset, E., Whitfield, M., & Touré, A. (2023).
592 CCDC65, encoding a component of the axonemal Nexin-Dynein regulatory complex,
593 is required for sperm flagellum structure in humans. *Clin Genet*, *105*(3), 317-322.
594 https://doi.org/10.1111/cge.14459
595 Kumar, N., & Singh, A. K. (2021). The anatomy, movement, and functions of human sperm
596 tail: an evolving mystery. *Biology of Reproduction*, *104*(3), 508-520.

https://doi.org/10.1093/biolre/ioaa213

Kumar, S., Stecher, G., Li, M., Knyaz, C., & Tamura, K. (2018). MEGA X: Molecular Evolutionary Genetics Analysis across Computing Platforms. *Mol Biol Evol*, *35*(6), 1547-1549. https://doi.org/10.1093/molbev/msy096

Lehti, M. S., & Sironen, A. J. B. o. r. (2017). Formation and function of sperm tail structures in association with sperm motility defects. *97*(4), 522-536. https://doi.org/10.1093/biolre/iox096

Lehti, M. S., & Sironen, A. J. R. (2016). Formation and function of the manchette and flagellum during spermatogenesis. *151*(4), R43-R54. https://doi.org/10.1530/REP-15-0310

Leung, M. R., Zeng, J., Wang, X., Roelofs, M. C., Huang, W., Zenezini Chiozzi, R., Hevler, J. F., Heck, A. J. R., Dutcher, S. K., Brown, A., Zhang, R., & Zeev-Ben-Mordehai, T. (2023). Structural specializations of the sperm tail. *Cell*, *186*(13), 2880-2896.e2817. https://doi.org/10.1016/j.cell.2023.05.026

Liska, F., Gosele, C., Rivkin, E., Tres, L., Cardoso, M. C., Domaing, P., Krejcí, E., Snajdr, P., Lee-Kirsch, M. A., de Rooij, D. G., Rooij, D. G., Kren, V., Krenová, D., Kierszenbaum, A. L., & Hubner, N. (2009). Rat hd mutation reveals an essential role of centrobin in spermatid head shaping and assembly of the head-tail coupling apparatus. *Biol. Reprod.*, *81*(6), 1196-1205. https://doi.org/10.1095/biolreprod.109.078980

Liu, G., Wang, N., Zhang, H., Yin, S., Dai, H., Lin, G., & Li, W. (2020). Novel mutations in PMFBP1, TSGA10 and SUN5: Expanding the spectrum of mutations that may cause acephalic spermatozoa. *Clin Genet*, *97*(6), 938-939. https://doi.org/10.1111/cge.13747

Liu, G., Xing, X., Zhang, H., Zhu, W., Lin, G., Lu, G., & Li, W. (2021). Patients with acephalic spermatozoa syndrome linked to novel TSGA10/PMFBP1 variants have favorable pregnancy outcomes from intracytoplasmic sperm injection. *Clin Genet*, *100*(3), 334-339. https://doi.org/10.1111/cge.14007

Lu, M., Kong, S., Xiang, M., Wang, Y., Zhang, J., Duan, Z., Zha, X., Wang, F., Cao, Y., & Zhu, F. (2021). A novel homozygous missense mutation of PMFBP1 causes acephalic

spermatozoa syndrome. *J Assist Reprod Genet*, *38*(4), 949-955. https://doi.org/10.1007/s10815-021-02075-7

Ma, A., Zhou, J., Ali, H., Abbas, T., Ali, I., Muhammad, Z., Dil, S., Chen, J., Huang, X., Ma, H., Zhao, D., Zhang, B., Zhang, Y., Shah, W., Shah, B., Murtaza, G., Iqbal, F., Khan, M. A., Khan, A., Li, Q., Xu, B., Wu, L., Zhang, H., & Shi, Q. (2023). Loss-of-function mutations in CFAP57 cause multiple morphological abnormalities of the flagella in humans and mice. *JCI Insight*, *8*(3), e166869. https://doi.org/10.1172/jci.insight.166869

Martinez, G., Beurois, J., Dacheux, D., Cazin, C., Bidart, M., Kherraf, Z. E., Robinson, D. R., Satre, V., Le Gac, G., Ka, C., Gourlaouen, I., Fichou, Y., Petre, G., Duliouist, E., Zouari, R., Thierry-Mieg, N., Touré, A., Arnoult, C., Bonhivers, M., Ray, P., & Coutton, C. (2020). Biallelic variants in MAATS1 encoding CFAP91, a calmodulin-associated and spoke-associated complex protein, cause severe astheno-teratozoospermia and male infertility. *J Med Genet*, *57*(10), 708-716. https://doi.org/10.1136/jmedgenet-2019-106775

Meng, X., Xu, C., Li, J., Qiu, B., Luo, J., Hong, Q., Tong, Y., Fang, C., Feng, Y., Ma, R., Shi, X., Lin, C., Pan, C., Zhu, X., Yan, X., & Cong, Y. (2024). Multi-scale structures of the mammalian radial spoke and divergence of axonemal complexes in ependymal cilia. *Nat Commun*, *15*(1), 362. https://doi.org/10.1038/s41467-023-44577-1

Nakata, H., Wakayama, T., Takai, Y., & Iseki, S. (2015). Quantitative analysis of the cellular composition in seminiferous tubules in normal and genetically modified infertile mice. *J Histochem Cytochem*, *63*(2), 99-113. https://doi.org/10.1369/0022155414562045

Nie, H., Tang, Y., Zhang, X., Tan, Y., & Qin, W. (2022). Novel mutations of PMFBP1 in a man with acephalic spermatozoa defects. *Mol Genet Genomic Med*, *10*(9), e2020. https://doi.org/10.1002/mgg3.2020

Parker, G. A. (2020). Conceptual developments in sperm competition: a very brief synopsis. *Philosophical Transactions of the Royal Society B-Biological Sciences*, *375*(1813), 20200061. https://doi.org/10.1098/rstb.2020.0061

Roldan, E. R. S. (2019). Sperm competition and the evolution of sperm form and function in mammals. *Reproduction in Domestic Animals*, *54*, 14-21. https://doi.org/10.1111/rda.13552

Saitou, N., & Nei, M. (1987). The neighbor-joining method: a new method for reconstructing phylogenetic trees. *Mol Biol Evol*, *4*(4), 406-425. https://doi.org/10.1093/oxfordjournals.molbev.a040454

Sha, Y. W., Wang, X., Xu, X., Ding, L., Liu, W. S., Li, P., Su, Z. Y., Chen, J., Mei, L. B., Zheng, L. K., Wang, H. L., Kong, S. B., You, M., & Wu, J. F. (2019). Biallelic mutations in PMFBP1 cause acephalic spermatozoa. *Clin Genet*, *95*(2), 277-286. https://doi.org/10.1111/cge.13461

Sha, Y. W., Xu, X., Ji, Z. Y., Lin, S. B., Wang, X., Qiu, P. P., Zhou, Y., Mei, L. B., Su, Z. Y., Li, L., & Li, P. (2018). Genetic contribution of SUN5 mutations to acephalic spermatozoa in Fujian China. *Gene*, *647*, 221-225. https://doi.org/10.1016/j.gene.2018.01.035

Shang, Y., Yan, J., Tang, W., Liu, C., Xiao, S., Guo, Y., Yuan, L., Chen, L., Jiang, H., Guo, X., Qiao, J., & Li, W. (2018). Mechanistic insights into acephalic spermatozoa syndrome-associated mutations in the human SUN5 gene. *J Biol Chem*, *293*(7), 2395-2407. https://doi.org/10.1074/jbc.RA117.000861

Shang, Y., Zhu, F., Wang, L., Ouyang, Y. C., Dong, M. Z., Liu, C., Zhao, H., Cui, X., Ma, D., Zhang, Z., Yang, X., Guo, Y., Liu, F., Yuan, L., Gao, F., Guo, X., Sun, Q. Y., Cao, Y., & Li, W. (2017). Essential role for SUN5 in anchoring sperm head to the tail. *Elife*, *6*, e28199. https://doi.org/10.7554/eLife.28199

Sudhakar, D. V. S., Shah, R., & Gajbhiye, R. K. (2021). Genetics of Male Infertility - Present and Future: A Narrative Review. *J Hum Reprod Sci*, *14*(3), 217-227. https://doi.org/10.4103/jhrs.jhrs_115_21

Tu, C. F., Wang, W. L., Hu, T. Y., Lu, G. X., Lin, G., & Tan, Y. Q. (2020). Genetic underpinnings of asthenozoospermia. *Best Practice & Research Clinical Endocrinology & Metabolism*, *34*(6), 101472. https://doi.org/10.1016/j.beem.2020.101472

Varadi, M., Anyango, S., Deshpande, M., Nair, S., Natassia, C., Yordanova, G., Yuan, D., Stroe, O., Wood, G., Laydon, A., Žídek, A., Green, T., Tunyasuvunakool, K., Petersen, S., Jumper, J., Clancy, E., Green, R., Vora, A., Lutfi, M., Figurnov, M., Cowie, A., Hobbs, N., Kohli, P., Kleywegt, G., Birney, E., Hassabis, D., & Velankar, S. (2022). AlphaFold Protein Structure Database: massively expanding the structural coverage of protein-sequence space with high-accuracy models. *Nucleic Acids Res*, *50*(D1), D439-d444. https://doi.org/10.1093/nar/gkab1061

Walton, T., Gui, M., Velkova, S., Fassad, M. R., Hirst, R. A., Haarman, E., O'Callaghan, C., Bottier, M., Burgoyne, T., Mitchison, H. M., & Brown, A. (2023). Axonemal structures reveal mechanoregulatory and disease mechanisms. *Nature*, *618*(7965), 625-633. https://doi.org/10.1038/s41586-023-06140-2

Wang, L., Tu, Z., Liu, C., Liu, H., Kaldis, P., Chen, Z., & Li, W. (2018). Dual roles of TRF1 in tethering telomeres to the nuclear envelope and protecting them from fusion during meiosis. *Cell Death Differ*, *25*(6), 1174-1188. https://doi.org/10.1038/s41418-017-0037-8

Wu, B., Gao, H., Liu, C., & Li, W. (2020). The coupling apparatus of the sperm head and tail†. *Biol Reprod*, *102*(5), 988-998. https://doi.org/10.1093/biolre/ioaa016

Xiang, M., Wang, Y., Wang, K., Kong, S., Lu, M., Zhang, J., Duan, Z., Zha, X., Shi, X., Wang, F., Cao, Y., & Zhu, F. (2022). Novel Mutation and Deletion in SUN5 Cause Male Infertility with Acephalic Spermatozoa Syndrome. *Reprod Sci*, *29*(2), 646-651. https://doi.org/10.1007/s43032-021-00665-5

Yuan, S., Stratton, C. J., Bao, J., Zheng, H., Bhetwal, B. P., Yanagimachi, R., & Yan, W. (2015). Spata6 is required for normal assembly of the sperm connecting piece and tight head-tail conjunction. *Proc Natl Acad Sci U S A*, *112*(5), E430-439. https://doi.org/10.1073/pnas.1424648112

Zamboni, L., & Stefanini, M. (1971). The fine structure of the neck of mammalian spermatozoa. *Anat Rec*, *169*(2), 155-172. https://doi.org/10.1002/ar.1091690203

Zhang, D., Huang, W. J., Chen, G. Y., Dong, L. H., Tang, Y., Zhang, H., Li, Q. Q., Mei, X. Y., Wang, Z. H., & Lan, F. H. (2021). Pathogenesis of acephalic spermatozoa syndrome

713 caused by SUN5 variant. *Mol Hum Reprod*, *27*(5), gaab028.
714 https://doi.org/10.1093/molehr/gaab028
715 Zhang, Y., Liu, C., Wu, B., Li, L., Li, W., & Yuan, L. (2021). The missing linker between
716 SUN5 and PMFBP1 in sperm head-tail coupling apparatus. *Nat Commun*, *12*(1),
717 4926. https://doi.org/10.1038/s41467-021-25227-w
718 Zhang, Y., Yang, L., Huang, L., Liu, G., Nie, X., Zhang, X., & Xing, X. (2021). SUN5
719 Interacting With Nesprin3 Plays an Essential Role in Sperm Head-to-Tail Linkage:
720 Research on Sun5 Gene Knockout Mice. *Front Cell Dev Biol*, *9*, 684826.
721 https://doi.org/10.3389/fcell.2021.684826
722 Zhou, L., Liu, H., Liu, S., Yang, X., Dong, Y., Pan, Y., Xiao, Z., Zheng, B., Sun, Y., Huang, P.,
723 Zhang, X., Hu, J., Sun, R., Feng, S., Zhu, Y., Liu, M., Gui, M., & Wu, J. (2023).
724 Structures of sperm flagellar doublet microtubules expand the genetic spectrum of
725 male infertility. *Cell*, *186*(13), 2897-2910.e2819.
726 https://doi.org/10.1016/j.cell.2023.05.009
727 Zhu, F., Liu, C., Wang, F., Yang, X., Zhang, J., Wu, H., Zhang, Z., He, X., Zhang, Z., Zhou, P.,
728 Wei, Z., Shang, Y., Wang, L., Zhang, R., Ouyang, Y. C., Sun, Q. Y., Cao, Y., & Li, W.
729 (2018). Mutations in PMFBP1 Cause Acephalic Spermatozoa Syndrome. *Am J Hum*
730 *Genet*, *103*(2), 188-199. https://doi.org/10.1016/j.ajhg.2018.06.010
731 Zhu, F., Wang, F., Yang, X., Zhang, J., Wu, H., Zhang, Z., Zhang, Z., He, X., Zhou, P., Wei,
732 Z., Gecz, J., & Cao, Y. (2016). Biallelic SUN5 Mutations Cause Autosomal-Recessive
733 Acephalic Spermatozoa Syndrome. *Am J Hum Genet*, *99*(6), 1405.
734 https://doi.org/10.1016/j.ajhg.2016.11.002
735

Figures and Figure legends

Fig. 1 CCDC113 is an evolutionarily conserved axoneme-associated protein. (A) Multiple species phylogenetic tree of CCDC113. Structural similarity scores (Z scores) of CCDC113 orthologs in *Homo sapiens*, *Mus musculus*, *Phascolarctos cinereus*, *Danio rerio*, *Chlamydomonas reinhardtii* and *Tetrahymena thermophila* were derived through the DALI webserver for pairwise structure comparisons (Holm & Laakso, 2016). (B) Positioning of CCDC113 within the 96-nm repeat of human axoneme (Walton et al., 2023). CCDC113 form a complex with CCDC96, is located at the base of RS3 and adjacent to CFAP91 and CFAP57. CFAP91 originates at the base of RS2 and links the RS3 subunits (CFAP251 and CFAP61). (C-H) Neighboring axoneme-associated proteins were expressed or co-expressed with CCDC113 in HEK293T cells, and the interactions of CCDC113 with CFAP57, CFAP91, TUBB5, DRC1, DRC2 and DRC3 were examined through co-immunoprecipitation. IB, immunoblotting; IP, immunoprecipitation.

Fig.2 *Ccdc113* knockout leads to male infertility. (A) The CRISPR-Cas9 strategy for generating the *Ccdc113* knockout mice. (B) Genotyping to identify *Ccdc113* knockout mice. (C) Immunoblotting of CCDC113 in *Ccdc113*$^{+/+}$ and *Ccdc113*$^{-/-}$ testes. TUBULIN served as the loading control. (D) The average litter size of *Ccdc113*$^{+/+}$ and *Ccdc113*$^{-/-}$ female mice in 2 months (n = 5 independent experiments). Data are presented as mean ± SD. ns: indicates no difference. (E) The average litter size of *Ccdc113*$^{+/+}$ and *Ccdc113*$^{-/-}$ male mice in 2 months (n = 5 independent experiments). Data are presented as mean ± SD. ****$P < 0.0001$. (F) The size of testes was similar in *Ccdc113*$^{+/+}$ and *Ccdc113*$^{-/-}$ mice. (G) The testis weights of *Ccdc113*$^{+/+}$ and *Ccdc113*$^{-/-}$ male mice (n = 5 independent experiments). Data are presented as mean ± SD. ns: indicates no difference. (H) The body weights of *Ccdc113*$^{+/+}$ and *Ccdc113*$^{-/-}$ male mice (n = 5 independent experiments). Data are presented as mean ± SD. ns: indicates no difference. (I) The ratio of testis weight/body weight in *Ccdc113*$^{+/+}$ and *Ccdc113*$^{-/-}$ male mice (n = 5 independent experiments). Data are presented as mean ± SD. ns: indicates no difference. (J) H&E staining of testes sections from *Ccdc113*$^{+/+}$ and *Ccdc113*$^{-/-}$ male mice. Red arrowheads indicate the abnormal sperm flagellum in the *Ccdc113*$^{-/-}$ testis seminiferous

tubule. (K) Immunofluorescence of acetylated-tubulin (red) in testes sections from *Ccdc113*$^{-/-}$ male mice show flagellar defects.

Fig. 3 *Ccdc113* knockout results in sperm flagella defects and sperm head-tail detachment.

(A) H&E staining of the caudal epididymis from *Ccdc113*$^{+/+}$ and *Ccdc113*$^{-/-}$ male mice in 2 months. Red circles indicate coiled eosin-stained structures without sperm heads in the epididymal lumen. (B) Analysis of sperm counts in *Ccdc113*$^{+/+}$ and *Ccdc113*$^{-/-}$male mice (n = 5 independent experiments). Mature spermatozoa were extracted from unilateral cauda epididymis and dispersed in PBS. Sperm counts were measured by hemocytometers. Data are presented as the mean ± SD. ****P < 0.0001. (C) Motile sperm in *Ccdc113*$^{+/+}$ and *Ccdc113*$^{-/-}$ mice (n = 5 independent experiments). Data are presented as mean ± SD. ****P < 0.0001. (D) *Ccdc113*$^{+/+}$ and *Ccdc113*$^{-/-}$ spermatozoa were co-stained with a flagellar marker α/β-tubulin (red) and an acrosomal marker PNA. Nuclei were stained with DAPI (blue). (E) Quantification of different categories of *Ccdc113*$^{+/+}$, *Ccdc113*$^{-/-}$ spermatozoa (n = 3 independent experiments). Data are presented as the mean ± SD.

Fig. 4. CCDC113 localizes to the HTCA, manchette and sperm flagellum. (A) CCDC113 was predominately expressed in testis and slightly in lung. Immunoblotting of CCDC113 was performed in the spleen, intestine, lung, thymus, testis and ovary. Asterisks indicate unspecific bands. TUBULIN served as the loading control. (B) CCDC113 was expressed starting in P7 testes. TUBULIN served as the loading control. Asterisks indicate unspecific bands. (C) Immunofluorescence of CCDC113 (red) and CENTRIN1/2 (green) in developing germ cells. CCDC113 partially colocalize with centriolar protein CENTRIN1/2. (D) Immunofluorescence of CCDC113 (red) and α/β-tubulin (green) in developing germ cells. The manchette was stained with the anti-α/β-tubulin antibody. (E-F) CCDC113 localizes to the HTCA and flagellum in mature mouse spermatozoa and human spermatozoa. Nuclei were stained with DAPI (blue).

Fig. 5 CCDC113 is indispensable for the docking of CFAP91 and DRC2 to the DMTs to maintain the structural integrity of the axoneme. (A) Transmission electron microscopy (TEM) analysis of spermatozoa from the cauda epididymidis of *Ccdc113*$^{+/+}$ and *Ccdc113*$^{-/-}$ male mice. The flagellar longitudinal sections of *Ccdc113*$^{-/-}$ spermatozoa revealed unremoved cytoplasm, including disrupted mitochondria, damaged axonemes. and large vacuoles. Asterisks indicate large vacuoles. Cross sections of the principal piece of *Ccdc113*$^{-/-}$ spermatozoa further revealed partial loss or unidentifiable "9+2" structures, along with the disruption of the fibrous sheath and outer dense fibers. (B) Transmission electron microscopy (TEM) analysis of the axoneme in testicular spermatids from *Ccdc113*$^{+/+}$ and *Ccdc113*$^{-/-}$ male mice. The red arrowheads indicate the absence of significant radial spokes (RSs). MS: mitochondrial sheath, Mi: mitochondrial, AX: axoneme. FS: fibrous sheath. DMT: doublet microtubule, MT: microtubule, CP: central pair, ODF: outer dense fiber, RS: radial spokes. (C) The immunofluorescence analysis for CFAP91 (green) and α/β-tubulin (red) was performed in *Ccdc113*$^{+/+}$ and *Ccdc113*$^{-/-}$ spermatozoa. Nuclei were stained with DAPI (blue). White asterisks indicate regions that are not co-located with tubulin. (D) The immunofluorescence analysis for DRC2 (green) and α/β-tubulin (red) was performed in *Ccdc113*$^{+/+}$ and *Ccdc113*$^{-/-}$ spermatozoa. Nuclei were stained with DAPI (blue). White asterisks indicate regions that are not colocated with tubulin. (E-F) Line-scan analysis (white line) using the Image J software.

Fig. 6 *Ccdc113* knockout spermatids display impaired HTCA. (A) The proportion of decapitated tails in *Ccdc113*$^{+/+}$ and *Ccdc113*$^{-/-}$ corpus, caput and cauda epididymis (n=3 independent experiments). Data are presented as the mean ± SD. ****P < 0.0001. ***P < 0.001. (B) PAS staining of testes sections from *Ccdc113*$^{+/+}$ and *Ccdc113*$^{-/-}$ mice. The green arrows indicate the orientation of the sperm heads in stages V–VIII seminiferous epithelia. *Ccdc113*$^{-/-}$ sperm head could still be detected in stages IX–X seminiferous epithelia. P: pachytene spermatocyte, spz: spermatozoa, rSt: round spermatid, eSt: elongating spermatid, Z: zygotene spermatocyte, M: meiotic spermatocyte. (C) *Ccdc113*$^{-/-}$ spermatids lost their head orientation toward the basement membrane during spermiation in stages VII–VIII

seminiferous epithelia. L: lumen, B: basement membrane. (D) Defective HTCA formation in *Ccdc113*$^{-/-}$ spermatids. TEM analyses of the stepwise development of the HTCA were performed in *Ccdc113*$^{+/+}$ and *Ccdc113*$^{-/-}$ testes. In *Ccdc113*$^{+/+}$ spermatids, the well-defined coupling apparatus was tightly attached to the sperm head. In *Ccdc113*$^{-/-}$ spermatids, segmented columns (Scs), the capitulum (Cp) were absent. The red asterisks indicate the distance between the sperm head and HTCA. The white arrows indicate the dense material surrounding the proximal centriole. Nu: nuclear, Bp: basal plate, Cp: capitulum, Sc: segmented column, Pc: proximal centriole, Dc: distal centriole, An: annulus, Ax: axoneme, Rn: redundant nuclear envelope.

Fig. 7 CCDC113 interact with SUN5 and CENTLEIN, participating in sperm head-tail linkage. (A-C, F) HTCA-associated proteins (SUN5, CENTLEIN, PMFBP1, SPATA6) were expressed or co-expressed with CCDC113 in HEK293T cells, and the interactions of CCDC113 with SUN5, CENTLEIN were examined through co-immunoprecipitation. CCDC113 did not interact with PMFBP1 and SPATA6. IB, immunoblotting; IP, immunoprecipitation. (D) SUN5 interacted CCDC113. pCDNA-FLAG-*Ccdc113* and pEGFP-GFP-*Sun5* were transfected into HEK293T cells. At 48 h after transfection, the cells were collected for immunoprecipitation (IP) with anti-GFP antibody and analyzed with anti-FLAG and anti-GFP antibodies. (E) CENTLEIN interacted CCDC113. pCMV-FLAG-*Centlein* and pEGFP-GFP-*Sun5* were transfected into HEK293T cells. At 48 h after transfection, the cells were collected for immunoprecipitation (IP) with anti-FLAG antibody and analyzed with anti-FLAG and anti-GFP antibodies. (G) Immunofluorescence of CCDC113 (red) and SUN5 (green) in mature spermatozoa. Nuclei were stained with DAPI (blue). (H) Immunofluorescence of CCDC113 (red) and CENTLEIN (green) in testicular step13-step14 spermatid. Nuclei were stained with DAPI (blue). (I) Immunofluorescence analysis for SPATA6 (green) and α/β-tubulin (red) was performed in *Ccdc113*$^{+/+}$ and *Ccdc113*$^{-/-}$ spermatozoa. Nuclei were stained with DAPI (blue). (J) Quantification ratio of SPATA6 on the detached sperm tail (n =3 independent experiments). At least 200 spermatozoa *were analyzed* for *each mouse.* (K) Quantification ratio of CCDC113 on the detached sperm tail (n

852 =3 independent experiments). At least 200 spermatozoa *were analyzed* for *each mouse.* (L)
853 Immunofluorescence analysis for CCDC113 (red) was performed in wild type (WT), *Sun5*$^{-/-}$
854 and *Centlein*$^{-/-}$ spermatozoa. Nuclei were stained with DAPI (blue).

Figure 1

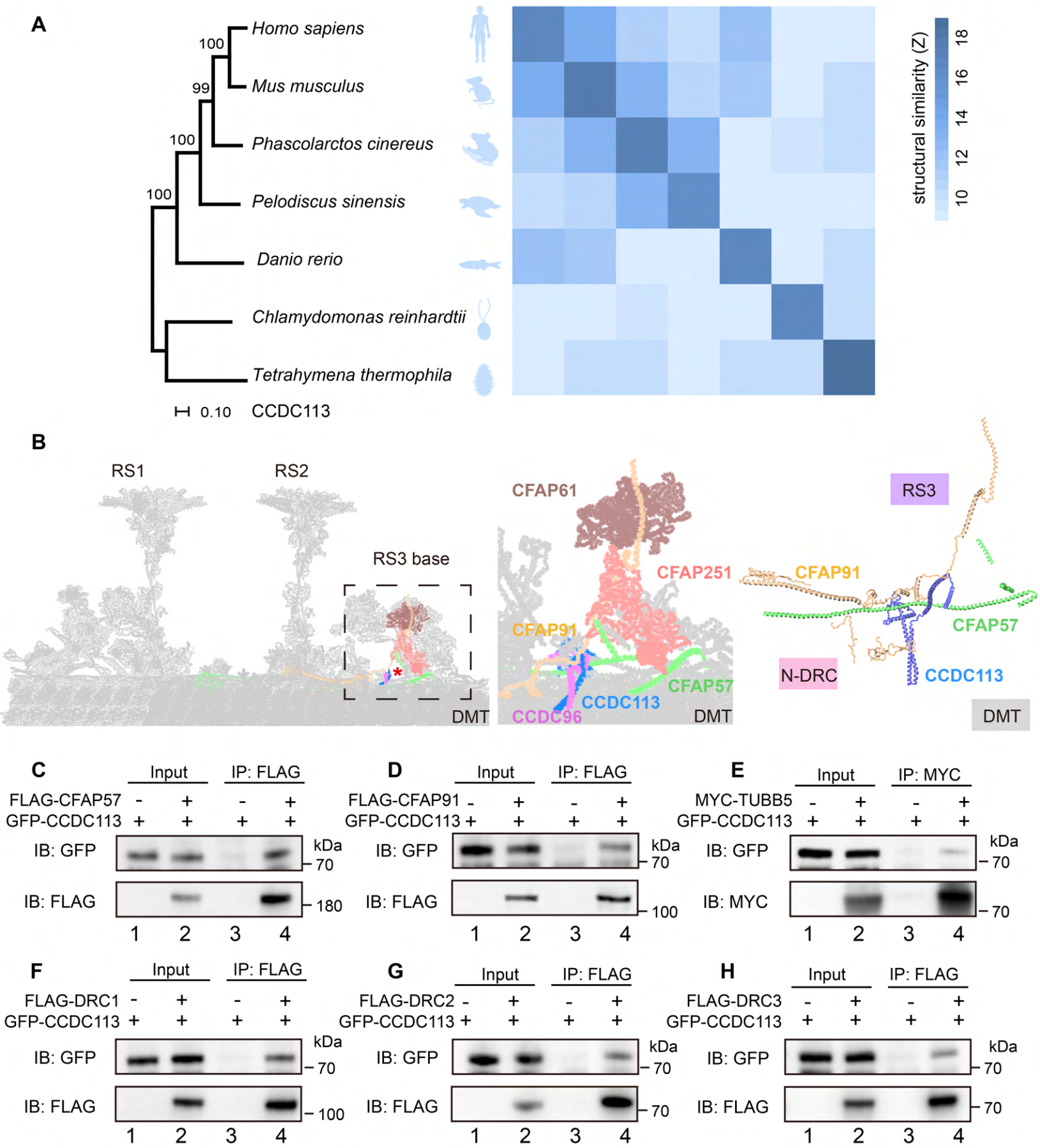
A
Homo sapiens
Mus musculus
Phascolarctos cinereus
Pelodiscus sinensis
Danio rerio
Chlamydomonas reinhardtii
Tetrahymena thermophila
100
99
100
100
0.10
CCDC113
structural similarity (Z)
18
16
14
12
10
B
RS1
RS2
RS3 base
DMT
CFAP61
CFAP251
CFAP91
CFAP57
CCDC113
CCDC96
DMT
RS3
CFAP91
CFAP57
N-DRC
CCDC113
DMT
C
Input
IP: FLAG
FLAG-CFAP57 - + - +
GFP-CCDC113 + + + +
IB: GFP
IB: FLAG
kDa
70
180
1 2 3 4
D
Input
IP: FLAG
FLAG-CFAP91 - + - +
GFP-CCDC113 + + + +
IB: GFP
IB: FLAG
kDa
70
100
1 2 3 4
E
Input
IP: MYC
MYC-TUBB5 - + - +
GFP-CCDC113 + + + +
IB: GFP
IB: MYC
kDa
70
70
1 2 3 4
F
Input
IP: FLAG
FLAG-DRC1 - + - +
GFP-CCDC113 + + + +
IB: GFP
IB: FLAG
kDa
70
100
1 2 3 4
G
Input
IP: FLAG
FLAG-DRC2 - + - +
GFP-CCDC113 + + + +
IB: GFP
IB: FLAG
kDa
70
70
1 2 3 4
H
Input
IP: FLAG
FLAG-DRC3 - + - +
GFP-CCDC113 + + + +
IB: GFP
IB: FLAG
kDa
70
70
1 2 3 4

Figure 2

A

44.81kb

Primer F1 Primer F2 Primer R

Ccdc113

Exon1 2 3 4 5 6 7 8 9

Ccdc113 $^{+/+}$ AAGGCAAGGGAAGTATCTAGAGATGGTCGGTGGG----CTTATCGGGGGTGAGGGACACAGATCTGGC

Ccdc113 $^{-/-}$ AAGGCAAGGGAAGTATCTAGAGATGG--- 10215bp --- GTCAGGGTGGGAATACAGTACAGACACATGT
GTTCAAATGGGGGAAGCTCCCAGGTGTGCCTCCCTTATCGGGGGTGAGGGACACAGATCTGGC

B

F1/R 539bp

F2/R 461bp

Ccdc113 $^{+/+}$ *Ccdc113* $^{-/-}$ *Ccdc113* $^{+/-}$

C

kDa

CCDC113 50 40

TUBULIN 55

Ccdc113 $^{+/+}$ *Ccdc113* $^{-/-}$

D

Female fertility

ns

Average litter size 0 6 12

Ccdc113 $^{+/+}$ *Ccdc113* $^{-/-}$

E

Male fertility

****

Average litter size 0 6 12

Ccdc113 $^{+/+}$ *Ccdc113* $^{-/-}$

F

Ccdc113 $^{+/+}$ *Ccdc113* $^{-/-}$

G

ns

Testis weight (g) 0.00 0.06 0.12

Ccdc113 $^{+/+}$ *Ccdc113* $^{-/-}$

H

ns

Body weight (g) 0 10 20 30 40

Ccdc113 $^{+/+}$ *Ccdc113* $^{-/-}$

I

ns

Testis weight/body weight 0.000 0.001 0.002 0.003 0.004

Ccdc113 $^{+/+}$ *Ccdc113* $^{-/-}$

J

Ccdc113 $^{+/+}$

Ccdc113 $^{-/-}$

100μm 50μm 100μm 50μm

K

DAPI ac-TUBULIN MERGE

Ccdc113 $^{+/+}$

Ccdc113 $^{-/-}$

10μm 10μm

Figure 3

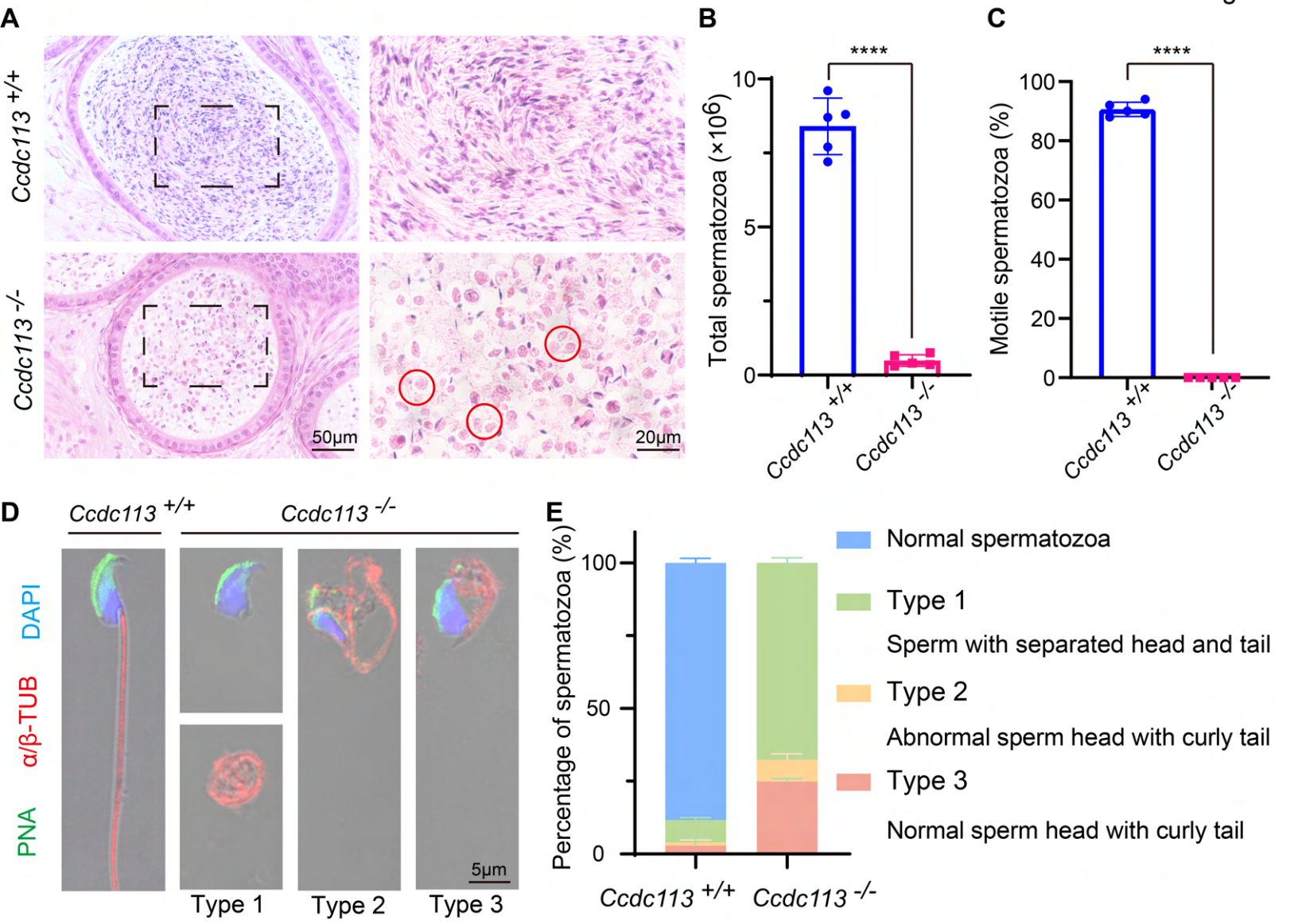
A
Ccdc113 +/+
Ccdc113 -/-
50μm
20μm
B
Total spermatozoa (×10^6)
10
5
0
****
Ccdc113 +/+
Ccdc113 -/-
C
Motile spermatozoa (%)
100
80
60
40
20
0
****
Ccdc113 +/+
Ccdc113 -/-
D
Ccdc113 +/+
Ccdc113 -/-
DAPI
α/β-TUB
PNA
5μm
Type 1
Type 2
Type 3
E
Percentage of spermatozoa (%)
100
50
0
Ccdc113 +/+
Ccdc113 -/-
Normal spermatozoa
Type 1
Sperm with separated head and tail
Type 2
Abnormal sperm head with curly tail
Type 3
Normal sperm head with curly tail

Figure 4

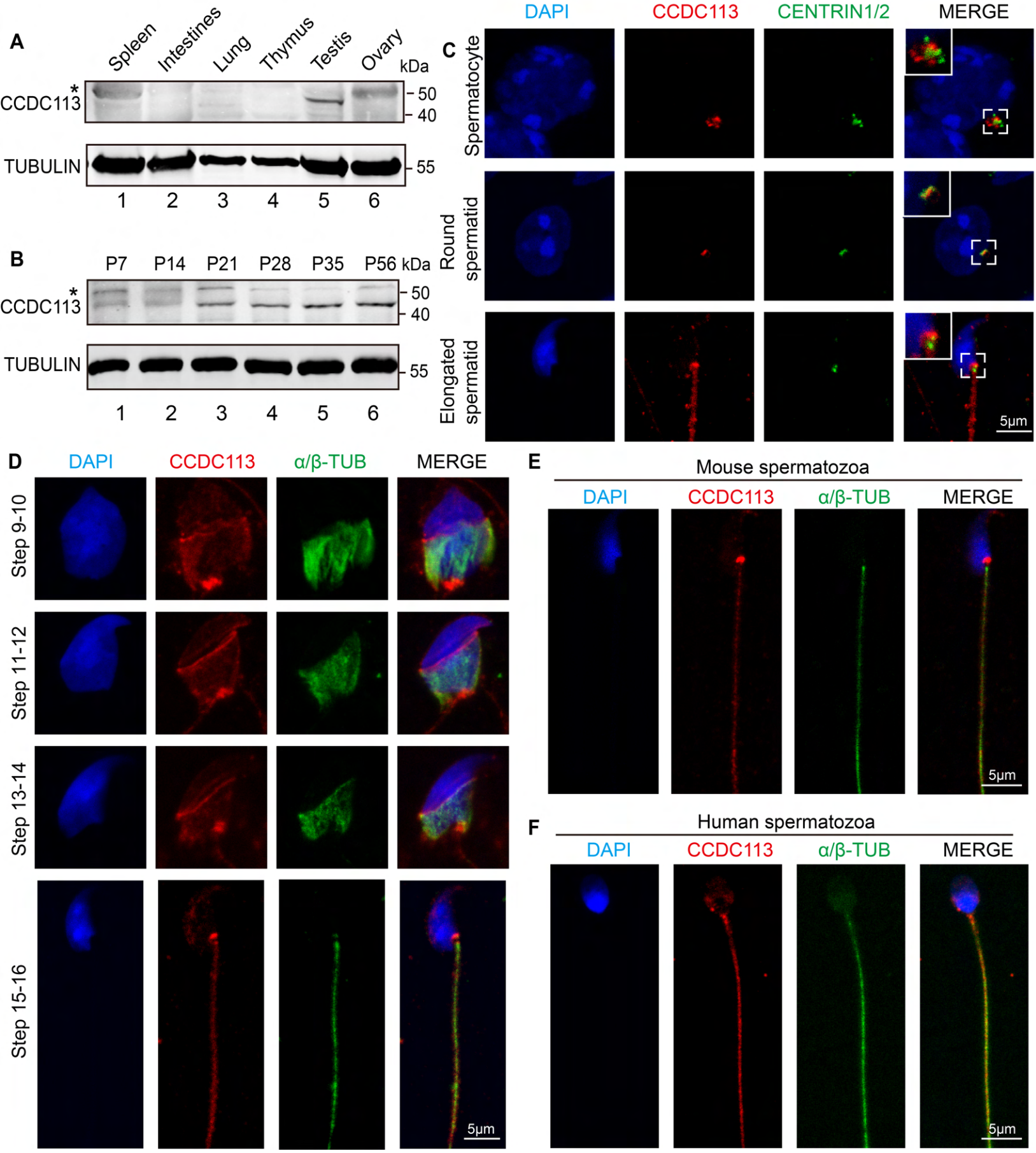
A
Spleen
Intestines
Lung
Thymus
Testis
Ovary
kDa
CCDC113*
50
40
TUBULIN
55
1 2 3 4 5 6
B
P7 P14 P21 P28 P35 P56 kDa
CCDC113*
50
40
TUBULIN
55
1 2 3 4 5 6
C
DAPI
CCDC113
CENTRIN1/2
MERGE
Spermatocyte
Round spermatid
Elongated spermatid
5μm
D
DAPI
CCDC113
α/β-TUB
MERGE
Step 9-10
Step 11-12
Step 13-14
Step 15-16
5μm
E
Mouse spermatozoa
DAPI
CCDC113
α/β-TUB
MERGE
5μm
F
Human spermatozoa
DAPI
CCDC113
α/β-TUB
MERGE
5μm

Figure 5

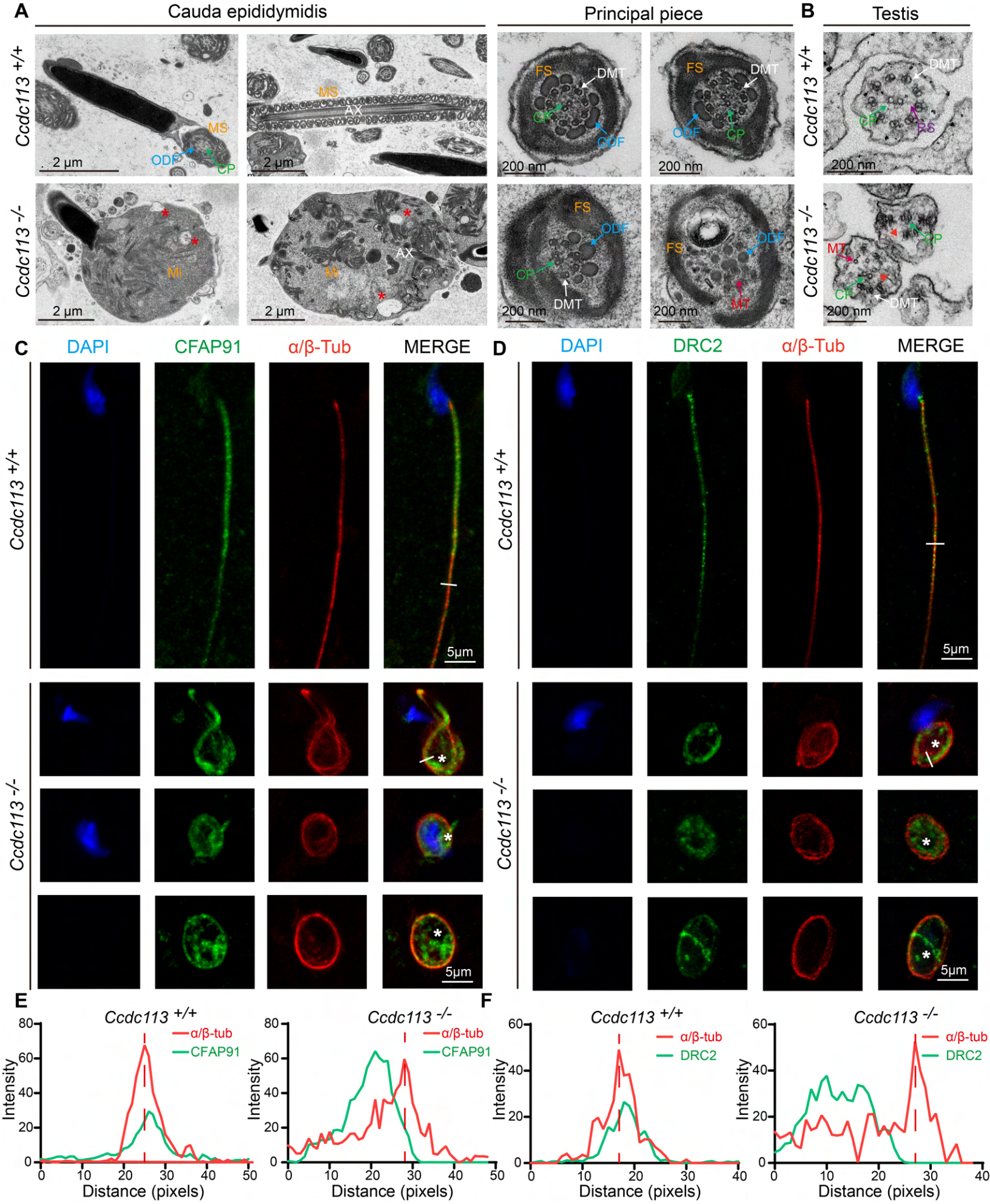
A
Cauda epididymidis
Principal piece
B
Testis
Ccdc113 +/+
Ccdc113 -/-
MS
AX
ODF
CP
FS
DMT
RS
MT
Mi
2 µm
200 nm
C
DAPI
CFAP91
α/β-Tub
MERGE
D
DRC2
5µm
E
α/β-tub
CFAP91
Intensity
Distance (pixels)
F
DRC2

Figure 6

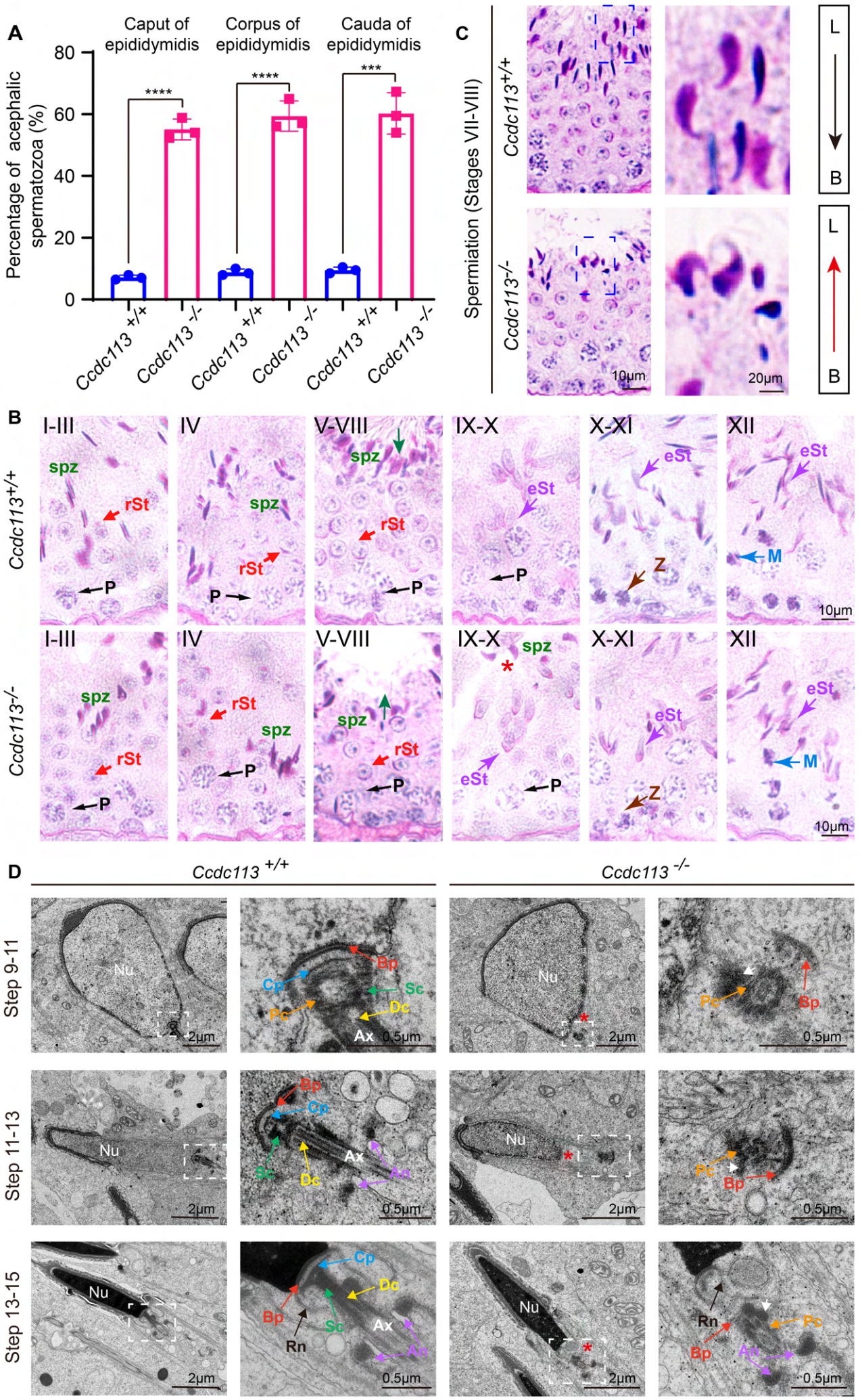
A
Caput of epididymidis
Corpus of epididymidis
Cauda of epididymidis
Percentage of acephalic spermatozoa (%)
80
60
40
20
0
****
****
***
Ccdc113 +/+
Ccdc113 -/-
C
Spermiation (Stages VII-VIII)
Ccdc113+/+
Ccdc113-/-
L
B
10μm
20μm
B
I-III
IV
V-VIII
IX-X
X-XI
XII
spz
rSt
P
eSt
Z
M
10μm
D
Ccdc113 +/+
Ccdc113 -/-
Step 9-11
Step 11-13
Step 13-15
Nu
Bp
Cp
Sc
Dc
Pc
Ax
An
Rn
2μm
0.5μm

Figure 7

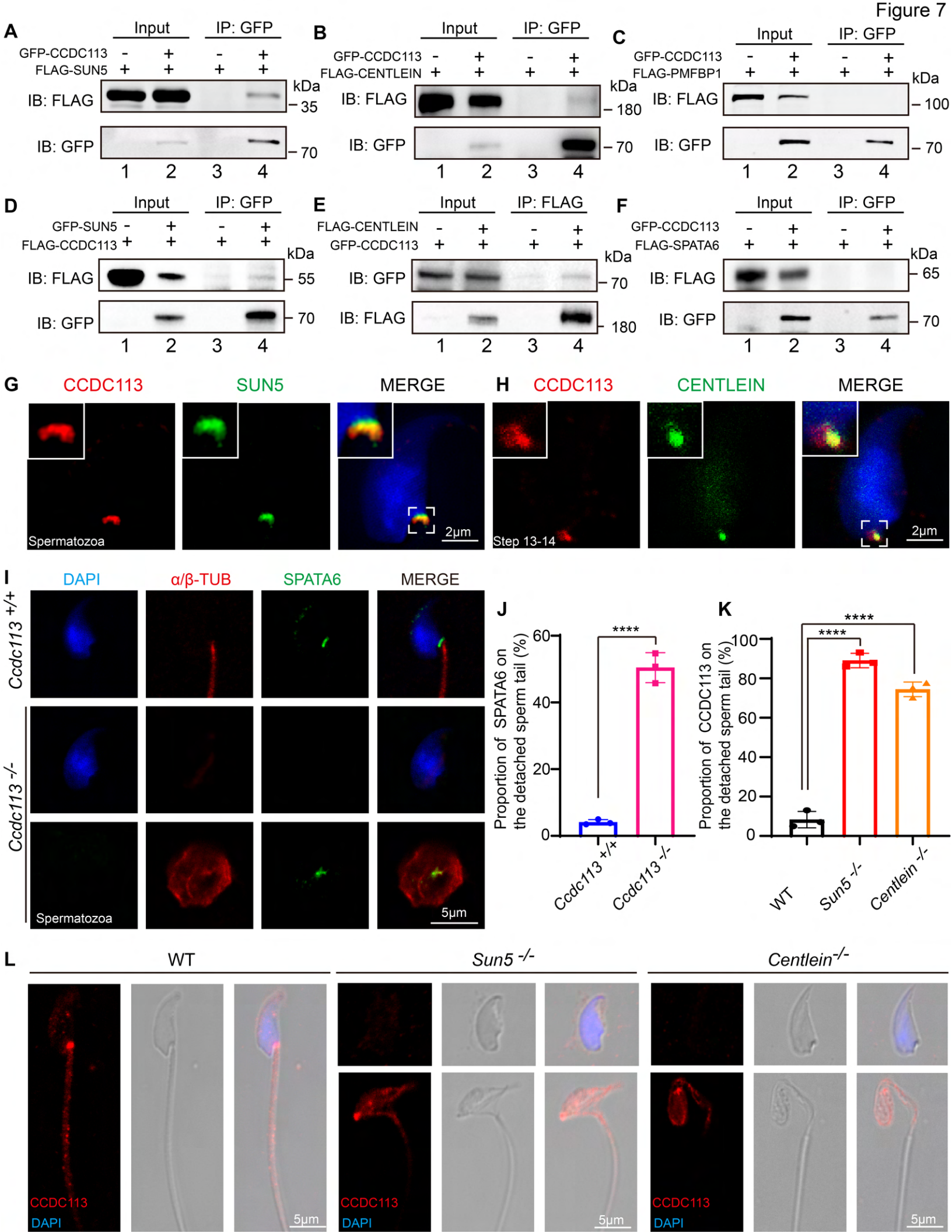
A
Input
IP: GFP
GFP-CCDC113 - + - +
FLAG-SUN5 + + + +
IB: FLAG
IB: GFP
kDa
35
70
1 2 3 4
B
Input
IP: GFP
GFP-CCDC113 - + - +
FLAG-CENTLEIN + + + +
IB: FLAG
IB: GFP
kDa
180
70
1 2 3 4
C
Input
IP: GFP
GFP-CCDC113 - + - +
FLAG-PMFBP1 + + + +
IB: FLAG
IB: GFP
kDa
100
70
1 2 3 4
D
Input
IP: GFP
GFP-SUN5 - + - +
FLAG-CCDC113 + + + +
IB: FLAG
IB: GFP
kDa
55
70
1 2 3 4
E
Input
IP: FLAG
FLAG-CENTLEIN - + - +
GFP-CCDC113 + + + +
IB: GFP
IB: FLAG
kDa
70
180
1 2 3 4
F
Input
IP: GFP
GFP-CCDC113 - + - +
FLAG-SPATA6 + + + +
IB: FLAG
IB: GFP
kDa
65
70
1 2 3 4
G
CCDC113
SUN5
MERGE
Spermatozoa
2μm
H
CCDC113
CENTLEIN
MERGE
Step 13-14
2μm
I
DAPI
α/β-TUB
SPATA6
MERGE
Ccdc113 +/+
Ccdc113 -/-
Spermatozoa
5μm
J
Proportion of SPATA6 on the detached sperm tail (%)
60
40
20
0
****
Ccdc113 +/+
Ccdc113 -/-
K
Proportion of CCDC113 on the detached sperm tail (%)
100
80
60
40
20
0
****
****
WT
Sun5 -/-
Centlein -/-
L
WT
Sun5 -/-
Centlein-/-
CCDC113
DAPI
5μm
CCDC113
DAPI
5μm
CCDC113
DAPI
5μm